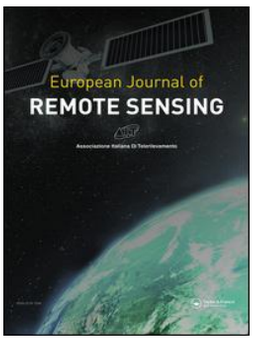

European Journal of Remote Sensing

ISSN: (Print) 2279-7254 (Online) Journal homepage: http://www.tandfonline.com/loi/tejr20

^{3}CAT-2: Attitude Determination and Control System for a GNSS-R Earth Observation 6U CubeSat Mission

Alexandre Cortiella, David Vidal, Jaume Jané, Enric Juan, Roger Olivé, Adrià Amézaga, Joan Francesc Munoz, Pol Via Hugo Carreno-Luengo & Adriano Camps

To cite this article: Alexandre Cortiella, David Vidal, Jaume Jané, Enric Juan, Roger Olivé, Adrià Amézaga, Joan Francesc Munoz, Pol Via Hugo Carreno-Luengo & Adriano Camps (2016) ^{3}CAT-2: Attitude Determination and Control System for a GNSS-R Earth Observation 6U CubeSat Mission, European Journal of Remote Sensing, 49:1, 759-776

To link to this article: http://dx.doi.org/10.5721/EuJRS20164940

Published online: 17 Feb 2017.

European Journal of Remote Sensing - 2016, 49: 759-776
doi: 10.5721/EuJRS20164940
Received 16/03/2016 accepted 01/09/2016

European Journal of Remote Sensing
An official journal of the Italian Society of Remote Sensing
www.aitjournal.com

[3]CAT-2: Attitude Determination and Control System for a GNSS-R Earth Observation 6U CubeSat Mission

Alexandre Cortiella*, David Vidal, Jaume Jané, Enric Juan, Roger Olivé, Adrià Amézaga, Joan Francesc Munoz, Pol Via Hugo Carreno-Luengo and Adriano Camps

Universitat Politècnica de Catalunya, Barcelona Tech Dept. of Signal Theory and Communications, UPC Campus Nord, D3; 08034 Barcelona, Spain
*Corresponding author, e-mail address: alexandre.cortiella@gmail.com

Abstract
This work describes the attitude determination and control system (ADCS) of [3]CAT-2, a six-unit CubeSat scheduled for launch this 2016. The ADCS of [3]CAT-2 aims at controlling the satellite in orbit and fulfilling the pointing requirements imposed by the mission. The attitude control system implemented in [3]CAT-2 will be used to point the antennas towards the Earth to perform altimetry tests, orient the solar panels towards the Sun to maximize power input when battery levels are critical, and reduce the tumbling motion of the satellite after the deployment phase. In order to guarantee pointing requirements for remote sensing purposes, an active three-axis attitude determination and control system is considered.

Keywords: Cat-2, nanosatellite, Cubesat, attitude determination and control, magnetic control, spacecraft dynamics.

Introduction
[3]Cat-2 cubesat is a research project conducted at Universitat Politècnica de Catalunya aiming at exploring novel GNSS-R techniques, acquire data over different targets to derive algorithms to infer geophysical parameters and demonstrate the reliability of nanosatellites for Earth Observation missions [Carreno-Luengo et al., 2015]. These goals require pointing accuracies up to 7.5º (3σ) for the nadir pointing operating mode. Passive attitude stabilization methods, such as magnetic or gravity gradient stabilization, have been successfully used in the past. However, these methods provide low pointing accuracy and are generally used for a single operating mode [Larson and Wertz, 1992]. Hence, a 3-axis active attitude control strategy is necessary to guarantee that the requirements of the mission are accomplished.
The proposed solution for dealing with pointing performance and controllability of [3]CAT-2 consists of three primary states of operation: nadir pointing, Sun tracking and detumbling. The first two are based on proportional-derivative (PD) control laws [Wie et al., 1989], whereas the third one uses the so-called B-dot algorithm which takes into account the local derivative of the magnetic field to dissipate the rotational energy from the satellite [Silani and Lovera, 2005].

The attitude control solution adopted for 3Cat-2 is based on a fully magnetic actuation achieved by a set of three orthogonal magnetorquer system - a combination of two torque rods and one air core torque providing 0.2 Am2 of magnetic moment each one. The benefits of using magnetic actuators are the low power consumption (1.2W in full actuation), low volume (~150 cm3) and low mass (~196 grams). Conversely, the major drawback is that the spacecraft control is instantaneously underactuated, and only the control torque perpendicular to the geomagnetic field vector can be provided. Fortunately, full controllability is guaranteed (on average) since the orbital inclination of the mission is nearly polar, and the direction of the geomagnetic field varies throughout the orbit [Silani and Lovera, 2005].

In conjunction with control, attitude determination plays a crucial role for feedback stabilization. The determination strategy implemented in 3Cat-2 includes a 3-axis rate gyroscope along with a fine 3-axis magnetometer enclosed in an Inertial Measurement Unit (IMU), one coarse 3-axis magnetometer integrated in the Onboard Computer, and 6 coarse silicon photodiodes attached on each face of the satellite. The determination algorithms included in 3Cat-2 are a computationally efficient version of the Extended Kalman Filter based on quaternion parameterization for the nominal mode, and the Quaternion Estimator (QUEST) algorithm for the Sun-safe mode. Attitude information is fed into the control algorithms to compute the error signal, and correct it by orienting the spacecraft to the desired attitude.

This paper is organized as follows: first, a brief summary of the reference frames and the spacecraft model, governed by the kinematic and dynamic Euler rigid body equations of motion, are presented. Second, an extensive presentation of the attitude determination and control system. This section is divided in four subsections: an introduction to the modes of operation, the attitude determination algorithms, the attitude control algorithms, and results from simulations. Thirdly, the testing facilities at the NanoSat Laboratory as well as the instrumentation to assess the performance and validate the overall ADCS of 3Cat-2 are presented. Finally, some conclusions are given evaluating the ADCS of the 3Cat-2 mission.

Spacecraft model

This section deals with the attitude dynamics that the spacecraft undergoes while orbiting around the Earth. The dynamic model adopted is based on an attitude quaternion parameterization for the kinematics, and the Euler's rigid body equations of motion for the dynamics. For the purpose of the present analysis, the following reference frames are considered:

- **Earth-Centered Inertial (ECI)** axes $\boldsymbol{F_i}$: the origin of this reference frame is located at the center of mass of the Earth. The X-axis points in the intersection between the ecliptic plane and the Earth's equatorial plane, and points towards the vernal equinox (Aries point). The Z-axis is aligned with the Earth's North Pole, and the Y-axis completes the right-handed triad.
- **Earth-Centered/Earth-Fixed (ECEF)** axes $\boldsymbol{F_e}$: as in the ECI reference frame, the origin of the ECEF frame is also located at the center of mass of the Earth and the Z-axis points in the direction of the Earth's North Pole. However, the X-axis points in the direction of the intersection of the Earth's Greenwich meridian and equator, and the Y-axis completes the right-handed system.

- **Orbital axes F_o**: the orbital frame adopted coincides with the Local-Vertical/Local-Horizontal (LVLH) reference frame. The origin is located at the center of mass of the satellite. The Z-axis coincides with the nadir vector (i.e. points towards the Earth's center of mass), the Y-axis points in the opposite direction of the orbit normal vector, and the X-axis completes the right-handed triad.
- **Body axes F_b**: this reference frame is attached to the satellite and is aligned with its geometrical axis. Its origin is located at the center of mass of the satellite. Figure 1 shows the body axis adopted. In case the inertia tensor were diagonal, then the principal inertia axis and the geometrical axis would coincide.

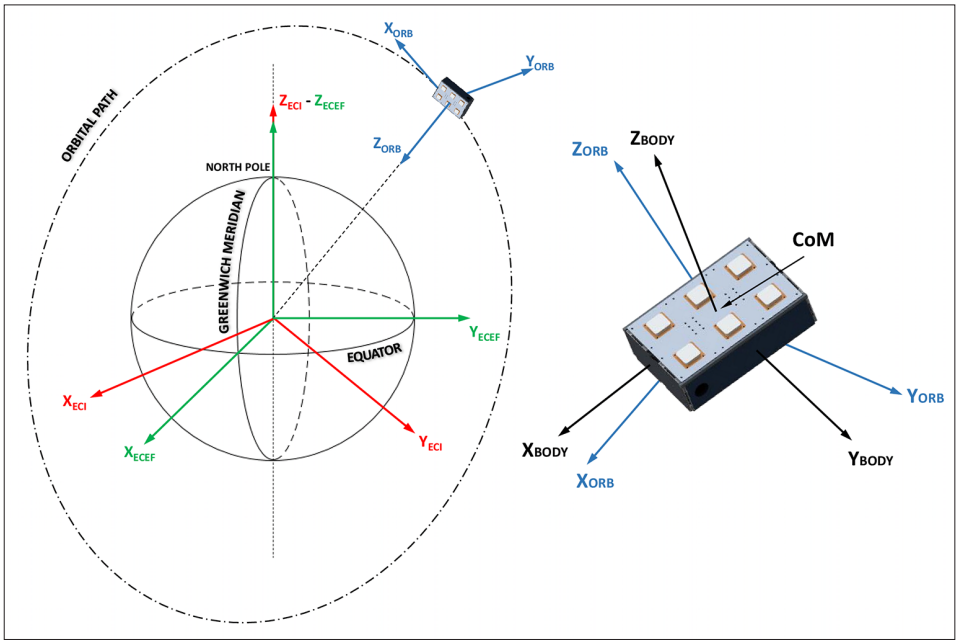

Figure 1 - Reference frames adopted for the spacecraft model.

For the kinematics, one of the most common attitude parameterizations is given by the four Euler parameters - or unit quaternions - due to its simplicity in computational implementation and because they are free of rotational sequences and nonsingular representations. The unit quaternion describes the orientation of one frame with respect to another by a set of four parameters and the unit norm constraint [Markley and Crassidis, 2014],

$$\mathbf{q} = (\mathbf{q}_v, q_4) = \left(\mathbf{e}\sin\left(\frac{\theta}{2}\right), \cos(\theta/2)\right) \in \mathbb{R}^4 \qquad [1]$$

where **e** denotes the unit vector representing the rotation axis (eigenaxis), and denotes the angle of rotation about **e** (Euler angle). A quaternion that represents a pure rotation must satisfy the unit norm constraint $\|\mathbf{q}\| = 1$, and the corresponding attitude matrix yields:

$$\mathbf{A}(\mathbf{q}) = (q_4^2 - \mathbf{q}_v^T\mathbf{q}_v)\mathbf{I}_{3\times3} + 2\mathbf{q}_v\mathbf{q}_v^T - 2q_4\left[\mathbf{q}_v^\times\right]^T \quad [2]$$

$\mathbf{I}_{3x3}$ denoting the identity matrix.
The quaternion kinematics can be described using quaternions as:

$$\dot{\mathbf{q}} = \frac{1}{2}\Xi(\mathbf{q})\omega \quad [3]$$

where $\omega \in \mathbb{R}^3$ is the spacecraft angular rate and $\Xi(\mathbf{q})$ is given by:

$$\Xi(\mathbf{q}) = \begin{bmatrix} q_4 & -q_3 & q_2 \\ q_3 & q_4 & -q_1 \\ -q_2 & q_1 & q_4 \\ -q_1 & -q_2 & -q_3 \end{bmatrix} \quad [4]$$

The attitude dynamics of a rigid body is described by the Euler's equations of motion:

$$\mathbf{I}\boldsymbol{\omega}_{bi}^b = -\boldsymbol{\omega}_{bi}^b \times \mathbf{I}\boldsymbol{\omega}_{bi}^b + \boldsymbol{\tau}_d^b + \boldsymbol{\tau}_c^b \quad [5]$$

where $\mathbf{I} \in \mathbb{R}^{3\times3}$ is the inertia tensor in the body frame F_b, $\boldsymbol{\omega}_{bi}^b$ is the spacecraft absolute angular rate, $\boldsymbol{\tau}_d^b$ is the sum of disturbance torques, and $\boldsymbol{\tau}_c^b$ is the control torque expressed in body frame.
Since the only actuators present in 3Cat-2 are a set of three orthogonal magnetorquers, then the control torque depends on the magnetic moment $\mathbf{m}_c^b$ generated by the coils, and the Earth's local magnetic field $\mathbf{b}^b$,

$$\boldsymbol{\tau}_c^b = \mathbf{m}_c^b \times \mathbf{b}^b \quad [6]$$

This expression clearly manifests that the control torque can only be generated on the plane perpendicular to the local Earth's magnetic field $\mathbf{b}^b$causing the system to be underactuated.
The external disturbance torques considered for the analysis are the gravity gradient $\left(\boldsymbol{\tau}_{gg}^b\right)$, aerodynamic $\left(\boldsymbol{\tau}_{aero}^b\right)$, solar radiation pressure $\left(\boldsymbol{\tau}_{rad}^b\right)$, and residual magnetic dipole torques $\left(\boldsymbol{\tau}_{mag}^b\right)$:

$$\boldsymbol{\tau}_d^b = \boldsymbol{\tau}_{gg}^b + \boldsymbol{\tau}_{aero}^b + \boldsymbol{\tau}_{rad}^b + \boldsymbol{\tau}_{mag}^b \quad [7]$$

The gravity gradient torque is caused by the Earth's gravitational field and tidal forces acting on the spacecraft. A simplified expression, assuming a spherical Earth as the only perturbing body, is given by [Hughes, 2004],

$$\boldsymbol{\tau}_{\mathbf{gg}}^{\mathbf{b}} = \frac{3\mu}{R^3}\hat{\mathbf{z}}_{\mathrm{ORB}} \times \mathbf{I}\hat{\mathbf{z}}_{\mathrm{ORB}} \quad [8]$$

where μ is the Earth's gravitational parameter, R is the spacecraft position with respect to the Earth's center of mass, and $\hat{\mathbf{z}}_{\mathrm{ORB}}$ is the unit vector pointing in the nadir direction. It is important to note that the dynamics under gravity gradient disturbances has 24 equilibrium points, some of them stable or unstable depending on the spacecraft's inertia tensor [Hughes, 2004]. The stable equilibrium is that one in which the axis of minimum moment of inertia points towards nadir, and the maximum moment opposite to the orbital plane normal.
The aerodynamic torque is caused by the atmospheric drag acting on the spacecraft's surfaces. The aerodynamic force model considered is a simplified one based on the drag coefficient C_D. Free molecular flow effects are not taken into account due to the difficulty to obtain accurate models and parameters. The expression of the torque is derived from the aerodynamic force:

$$\mathbf{f}_{\mathrm{aero}} = -\frac{1}{2}\rho v_r^2 C_D S(\hat{\mathbf{v}}_{\mathbf{r}} \cdot \hat{\mathbf{n}})\mathbf{v}_{\mathbf{r}} \quad [9]$$

where ρ is the local atmospheric density, $\mathbf{v}_{\mathbf{r}}$ is the spacecraft relative velocity with respect to the atmosphere, $\hat{\mathbf{n}}$ is the unit normal vector of each surface of the spacecraft, S is the area of each surface, and C_D is the drag coefficient, assumed 2.2 for this application [Franquiz et al., 2014]. In order to model the aerodynamic torque, the satellite is divided into 6 surfaces and the center of pressure (the point where $\mathbf{F}_{\mathrm{aero}}$ is acting) is assumed at the center of each surface. Hence the expression of the aerodynamic torque yields [Hughes, 2004]:

$$\boldsymbol{\tau}_{\mathrm{aero}}^{\mathbf{b}} = \sum_{f=1}^{6} \mathbf{r}_{\mathrm{cmp,f}}^{\mathrm{b}} \times \mathbf{f}_{\mathrm{aero,f}}^{\mathrm{b}} \Psi_f \quad [10]$$

where $\mathbf{r}_{\mathrm{cmp,f}}$ is the position vector of the center of pressure of the face **f** relative to the spacecraft center of mass, and $\Psi_f = \max\left(\left(\hat{\mathrm{v}}_r \cdot \hat{\mathrm{n}}\right), 0\right)$ is the shadowing function, since not all of the 6 faces are instantaneously wetted by the atmospheric flow.
The solar radiation force is produced by the exchange of momentum between the Sun's light and a surface of a body. The resulting solar radiation force is the balance between the incoming and outgoing momentum fluxes which can be modelled as:

$$\mathbf{f}_{\mathrm{rad}} = -\mathrm{PS}\left[2\left(\frac{\sigma_{\mathrm{rd}}}{3} + \sigma_{\mathrm{rs}}\hat{\mathbf{n}} \cdot \hat{\mathbf{s}}\right)\hat{\mathbf{n}} + \left(1 - \sigma_{\mathrm{rs}}\right)\hat{\mathbf{s}}\right] \quad [11]$$

where P is the solar momentum flux, S and $\hat{\mathbf{n}}$ are the area of the surface and its unit normal vector respectively, $\hat{\mathbf{s}}$ is the unit sun vector, and σ_{rs} and σ_{rd} are the coefficients of specular and diffuse reflection of the surface. As in the aerodynamic torque, the solar radiation pressure can be expressed as:

$$\boldsymbol{\tau}_{aero}^{b} = \sum_{f=1}^{6} \mathbf{r}_{cmp,f}^{b} \times \mathbf{f}_{rad,f}^{b} \Psi_{f} \quad [12]$$

Finally, the residual magnetic dipole torque is the torque caused by the residual dipoles generated by ferromagnetic materials or current loops in the spacecraft. The expression for the magnetic residual torque is the same as in Equation [6], but in this case the magnetic residual dipole moment is used:

$$\boldsymbol{\tau}_{mag}^{b} = \mathbf{m}_{res}^{b} \times \mathbf{b}^{b} \quad [13]$$

The satellite will operate in a polar Sun-Synchronous Orbit (SSO) with a Local Time of Ascending Node (LTAN) of 12:00 h (AM), and an orbit reference height of ~ 510 km [Carreno-Luengo et al., 2015]. Table 1 collects the expected maximum torques that the satellite will experience in orbit:

Table 1 - Maximum expected external torques on the ^{3}Cat-2 nanosatellite.

External torque	Maximum torque [Nm]
Gravity Gradient	$4.6 \cdot 10^{-8}$
Aerodynamic	$5.9 \cdot 10^{-8}$
Solar radiation	$6.6 \cdot 10^{-8}$
Magnetic residual	$1.9 \cdot 10^{-6}$
Magnetic control	$3.9 \cdot 10^{-4}$

Attitude determination and control for ^{3}Cat-2

The prime purpose of the attitude determination and control system is to control and stabilize the orientation of the satellite within a given tolerance about a desired attitude counteracting the external disturbances. This section introduces the ADCS modes of operation of ^{3}Cat-2, and gives an insight into the determination and control algorithms implemented.

Modes of operation

The attitude determination and control system of ^{3}Cat-2 has 3 main control modes -detumbling, Sun-safe and nominal - and one survival mode in case of failure. After the deployment from the launch vehicle, the satellite will tumble in an uncontrolled motion. The aim of the detumbling mode is to decrease the angular rate of the satellite from a maximum expected value of 10°/s to about 0.5°/s for subsequent control purposes. Then, the Sun-safe mode takes place and it aims at pointing the solar panels towards the Sun -within a tolerance of 20° (3σ) - so as to maximize the generation of electrical power from the Sun and charge the on-board batteries. Once the energy levels reach a certain level, then the nominal or nadir pointing mode goes into action. In this mode the six antenna array

is oriented in the nadir direction to collect the reflected navigation signals transmitted by GPS, Galileo or Beidou satellites [Carreno-Luengo et al., 2014] -within a pointing accuracy of 7.5° (3σ) - for scientific purposes. In terms of ADCS, the survival mode uses the same control algorithm as in the Sun-Safe mode, but switching off certain payloads to minimize energy consumption. This mode is accessed via ground station (GS) command when ADCS or command data handling (CDH) failures occur. Figure 2 illustrates the flow diagram of the different ADCS operating modes for 3Cat-2.

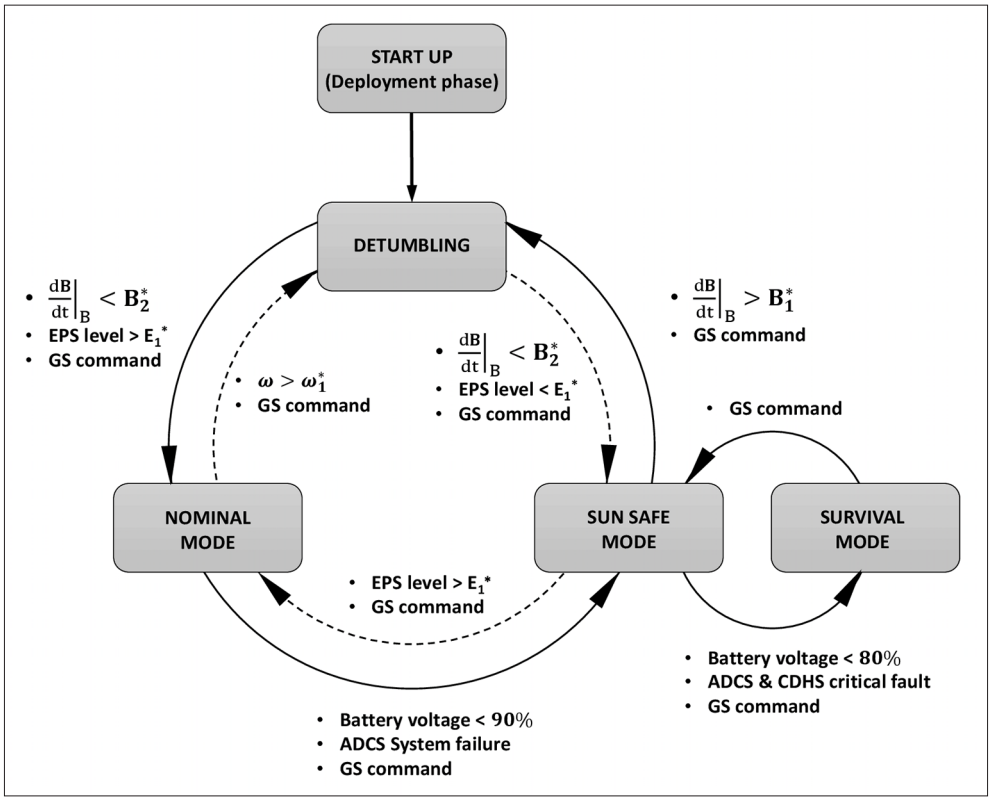

Figure 2 - Diagram of 3Cat-2 ADCS modes of operation.

Attitude determination

Attitude determination algorithms provide real-time or post-facto attitude knowledge by processing measurements from the on-board sensors. Three-axis attitude determination requires two or more vector observations, and are divided into static and state estimation techniques. For the 3Cat-2 mission, the nominal and Sun-Safe -and consequently Survival- operational modes are the only ones which use determination algorithms since they require attitude knowledge for pointing maneuvers.

On the one hand, the Sun-Safe mode employs 6 coarse silicon photodiodes and one coarse 3-axis magnetometer to determine the Sun's position and the spacecraft's angular rate. The attitude determination implemented for the Sun-Safe mode is a combination of the

commonly used Quaternion Estimator (QUEST) [Shuster and Oh, 1981] algorithm along with a low-pass filter to estimate the spacecraft's angular rate without using information from the gyroscopes. This solution was adopted as a tradeoff between pointing accuracy, and computational and power consumption, since this is a critical mode when the batteries run out of power.

The QUEST algorithm solves the Wabha's problem [Whaba, 1965], and its quaternion-based optimal solution given by Davensport's q-method [Shuster and Oh, 1981] in an efficient way. The problem consists of finding the optimal quaternion that minimizes the attitude error. It may be stated as follows:

$$\mathbf{q}^{*} = \min_{\mathbf{q}\in\mathbb{R}} \frac{1}{2}\sum_{m=1}^{M} \left\| \mathbf{A}(\mathbf{q})\mathbf{r}_m - \mathbf{s}_m \right\|^2 \quad [14]$$

The derivation of the entire algorithm can be found in [Markley and Crassidis, 2014]. The benefit of QUEST instead of q-method is that the optimal quaternion is obtained by solving a quartic equation instead of an eigenvalue problem, resulting in a computationally suitable method.

Once the attitude is computed, the angular rate can be estimated as,

$$\tilde{\boldsymbol{\omega}}_k = 2\Xi^{T}\left(\mathbf{q}_k\right)\dot{\mathbf{q}}_k \qquad k = 1,2,3... \quad [15]$$

where $\Xi^{T}(\mathbf{q})$ is given in Equation [4] and

$$\dot{\mathbf{q}}_k = \frac{\mathbf{q}_k - \mathbf{q}_{k-1}}{\Delta t} \qquad k = 1,2,3... \quad [16]$$

Since differentiation of noisy measurements amplifies noise, a low-pass filter is used after the angular rate estimation.

On the other hand, the nominal mode uses the same 6 photodiodes, one finer 3-axis magnetometer, and one 3-axis MEMS gyroscope to estimate the spacecraft's attitude and angular rate. In this mode, since the pointing accuracy is higher and the gyroscopes need to be corrected due to their drifts in the bias, a quaternion-based Extended Kalman Filter is employed. The essential feature of the Kalman filter is that it uses a mathematical model to predict an estimate of the attitude which is then corrected by the sensor measurements along with optimal statistical parameters taking into account state errors and zero-mean Gaussian noise. Another key feature is that it allows to merge several sensor measurements to obtain more accurate estimates. The Extended Kalman Filter selected for ^{3}Cat-2 is known as Multiplicative Extended Kalman Filter (MEKF) which hinges upon quaternions and their properties [Markley and Crassidis, 2014].

Further, the Murrell's version [Murrell, 1978] is considered, leading to an algorithmic structure which is computationally efficient and suitable for practical applications; the inverse of 3 by 3 matrices are computed N times instead of inverting 3N by 3N matrices. Figure 3 illustrates the MEKF adapted to the Murrell's structure.

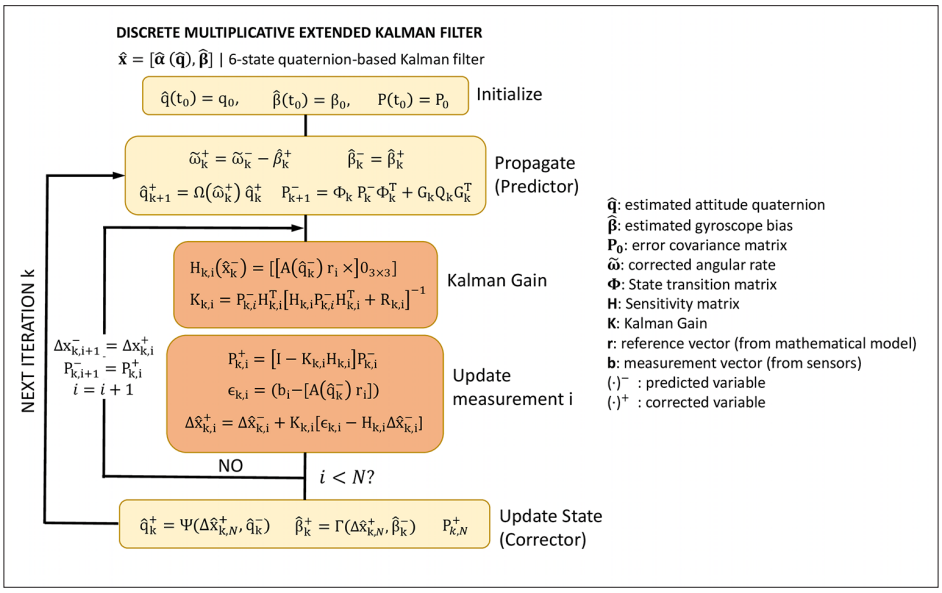

Figure 3 - Multiplicative Extended Kalman Filter with Murrell's structure. Adapted from [Crassidis and Junkins, 2011].

This version of the Extended Kalman Filter does not use models of rotational dynamics and torques (discussed in section "Attitude determination and control for 3Cat-2") nor information from the gyroscopes to update the measurements. Instead, gyroscope errors - such as noise and bias drifts - are corrected by means of other available on-board sensors. According to [Markley and Crassidis, 2014], this approach avoids corrupting gyro data from inaccurate dynamic models, and requires much less computational effort.

Attitude control

The control algorithms implemented in 3Cat-2 rely on simple control laws in order to reduce computational effort and complexity when implemented in a real-time On-Board Computer (OBC). Each mode of operation - detumbling, Sun-safe and nominal - has its own control law depending on their control purpose. As commented before, the only available control torque when using magnetic actuation is the one that lies in the plane perpendicular to the local geomagnetic field, as shown in Equation [6]. Therefore, the major drawback of this type of actuation is that the control is inherently underactuated, and causes controllability issues. Fortunately, as extensively studied in [Bhat and Dham, 2003], as long as the orbital plane does not coincide with the geomagnetic equatorial plane and does not contain the magnetic poles - this mission has an orbit inclination of ~98º-, the spacecraft is controllable on average throughout one revolution.

The control laws that will be presented for each mode are based on the projection of the ideal torque onto the plane perpendicular to the local geomagnetic field; thus, the parallel component is removed since it will not contribute to the applied torque. The projection of the ideal control torque, given by the control laws that will be discussed next, can be expressed as [Lovera and Astolfi, 2004]:

$$\boldsymbol{\tau}_{c}^{b} = \frac{1}{\left\|\mathbf{b}^{b}\right\|^{2}}\left[\mathbf{b}^{\times}\right]\left[\mathbf{b}^{\times}\right]^{T}\boldsymbol{\tau}_{c,ideal}^{b} \quad [17]$$

The detumbling mode uses a typical control law known as B-dot algorithm [Stickler and Alfried, 1976]. The aim of this controller is to dissipate rotational energy from the spacecraft to reduce it angular rate from a maximum expected value of 10º/s to about 0.5º/s without using gyroscope data. To accomplish this, the time derivative of the local geomagnetic field is computed as a derivative error which must be reduced. The B-dot control law is given by,

$$\mathbf{m}_{c}^{b} = -\mathbf{K}_{d,bdot}\dot{\mathbf{b}}^{b} \quad [18]$$

where $\mathbf{m}_{c}^{b}$ is the magnetic control moment, $\mathbf{K}_{d,bdot}$ is a positive-definite constant gain matrix and $\dot{\mathbf{b}}^{b}$ is the time-derivative of the local geomagnetic field measured by the on-board magnetometers. The time derivative $\dot{\mathbf{b}}^{b}$ may be easily computed with a first-order finite difference approach (15.2) along with a low-pass filter to reduce noise levels:

$$\dot{\mathbf{b}}_{k}^{b} \approx \frac{\mathbf{b}_{k}^{b} - \mathbf{b}_{k-1}^{b}}{\Delta t} \quad k = 1,2,3... \quad [19]$$

In agreement with [Avanzini and Giulietti, 2012], although global asymptotic stability to a zero absolute angular rate is not attainable by means of the considered control law (Eq. [18]), it is possible to reduce the spacecraft's angular rate to a value of the same order as the orbit rate (~0.06 º/s).

Both the Sun-safe and nominal modes use simple PD-like control laws due its implementation simplicity and reduced computational effort. The controller implemented in the Sun-safe mode follows a PD structure as well where the proportional term refers to the sun error vector, and the derivative term refers to the spacecraft's angular rate $\tilde{\boldsymbol{\omega}}$ estimated by the algorithm discussed in section "Attitude determination". The Sun-Safe control law is given by [Starin and Bourkland, 2007a],

$$\boldsymbol{\tau}_{ssc}^{b} = -\mathbf{K}_{p,ss}\hat{\mathbf{s}}_{e}^{b} - \mathbf{K}_{d,ss}\tilde{\boldsymbol{\omega}}^{b} \quad [20]$$

where the Sun error vector is the cross product between the unit sun vector and the unit Sun target (Eq. [21]), and $\mathbf{K}_{p,ss}$ and $\mathbf{K}_{d,ss}$ are constant gain diagonal matrices. The Sun target is defined as the axis of the spacecraft that is desired to point towards the Sun. In case of 3Cat-2, since the face of maximum area containing solar cells is the one which is opposite to the one containing the six-antenna array, the sun target vector is $\hat{\mathbf{s}}_{t} = [0,0,-1]$:

$$\hat{\mathbf{s}}_{e}^{b} = \hat{\mathbf{s}}^{b} \times \hat{\mathbf{s}}_{t}^{b} \quad [21]$$

When the spacecraft is in eclipse, then the Sun vector $\hat{\mathbf{s}}^{b}$ cannot be measured - and consequently the Sun error vector cannot be measured either. Therefore, the magnetorquers are disabled and no torque is generated until the spacecraft leaves the eclipse.
The aforementioned control law (Eq. [18]) has been proven to be globally, asymptotically stable for a fully controllable spacecraft in the absence of disturbance torques as long as the control gain matrices are positive definite [Starin and Bourkland, 2007b]. Since 3Cat-2 only employs magnetic actuation, the effectiveness of this control mode will be assessed through computer simulation.
Finally, the nominal mode also uses a simple PD-like control law but the proportional term contains the attitude error quaternion and the derivative term uses the relative spacecraft's angular rate (Eq. [22]). The attitude error quaternion relates the orientation of the body frame with respect to the LVLH orbital frame, and is defined in Equation [23] where $\mathbf{q}_{o}^{b}$ is the spacecraft's attitude quaternion estimated by the MEKF, and $\mathbf{q}_{t}$ is the target quaternion. Again, $\mathbf{K}_{p,n}$ and $\mathbf{K}_{d,n}$ are the proportional and derivative constant gain diagonal matrices respectively.

$$\boldsymbol{\tau}_{nc}^{b} = -\mathbf{K}_{p,n}\delta\mathbf{q}_{\boldsymbol{v}o}{}^{b} - \mathbf{K}_{d,n}\delta\boldsymbol{\omega}_{r}^{b} \quad [22]$$

$$\delta\mathbf{q}_{\boldsymbol{v}o}{}^{b} = \left(\mathbf{q}_{o}^{b} \otimes \mathbf{q}_{t}^{-1}\right)_{\boldsymbol{v}} \quad [23]$$

As we want to bring the spacecraft's z-axis to the z-axis of the orbital frame to point the antenna array in the nadir direction, the quaternion target must be $\mathbf{q}_{t}$=[0,0,0,1]. The relative angular rate term is the difference between the spacecraft's absolute angular rate vector and the orbital rate vector expressed in the body frame.

$$\delta\boldsymbol{\omega}_{r}^{b} = \boldsymbol{\omega}_{bi}^{b} - \mathbf{A}\left(\mathbf{q}_{o}^{b}\right)\boldsymbol{\omega}_{oi}^{o} \quad [24]$$

$$\boldsymbol{\omega}_{oi}^{o} = [0, -n, 0] \quad [25]$$

n being the magnitude of the orbit rate.
Several studies have discussed the stability conditions of the full state feedback control law given in Equations [22-25]. According to reference [Markley and Crassidis, 2014], the proposed control law is global, asymptotically stable in a torque free environment, and assuming that full control is available. Reference [Lovera and Astolfi, 2004] analyzes the effect of underactuation on a magnetically actuated spacecraft and concludes that attitude stabilization can be achieved in the absence of other active and passive stabilization techniques such as momentum wheels or gravity booms. Finally, references [Lovera and Astolfi, 2006] - [Reyhanoglu and Drakunov, 2009] include the effect of a favorable gravity gradient disturbance torque to bring the satellite to an Earth-pointing equilibrium, guaranteeing almost global stability. Nevertheless, 3Cat-2 mission requires the satellite to

point the antenna array - located in the face of maximum moment of inertia - in the nadir direction, leading to an unstable equilibrium point with respect to the gravity gradient torque. Furthermore, the rest of the disturbance torques discussed in section "Attitude determination and control for 3Cat-2", saturation of coils, noise and biases and other effects must be taken into account to assess the performance of the proposed control algorithms. For this reason, numerical simulations including all these effects were carried out.

Results

This section presents the results from several numerical simulations that were performed to reproduce the conditions at which the 3Cat-2 will be exposed once in orbit and assess the performance of the attitude determination and control system for each mode of operation. The following simulations were carried out using a SGP4 orbit propagator, an IGRF-12 Earth's magnetic field model, a Sun position algorithm, a conical eclipse model, a 5th order fixed step Runge-Kutta solver, and using the following inertia tensor,

$$\mathbf{I} = \begin{bmatrix} 0.0372 & -0.0007 & -0.001 \\ -0.0007 & 0.0703 & -0.0006 \\ -0.001 & -0.0006 & 0.0922 \end{bmatrix} \text{kg} \cdot \text{m}^2 \quad [26]$$

Detumbling control

The following figure (Fig. 4) represents the performance of the detumbling controller with random initial attitude and initial angular rate of 10º/s for each axis. As shown, the angular rate and the derivative of the Earth's local geomagnetic field progressively decreases (i.e. spacecraft's rotational energy) until reaching stability near zero value in less than one orbital period. After several simulations with different initial attitudes and control gains, the Bdot control law turns out to be very robust.

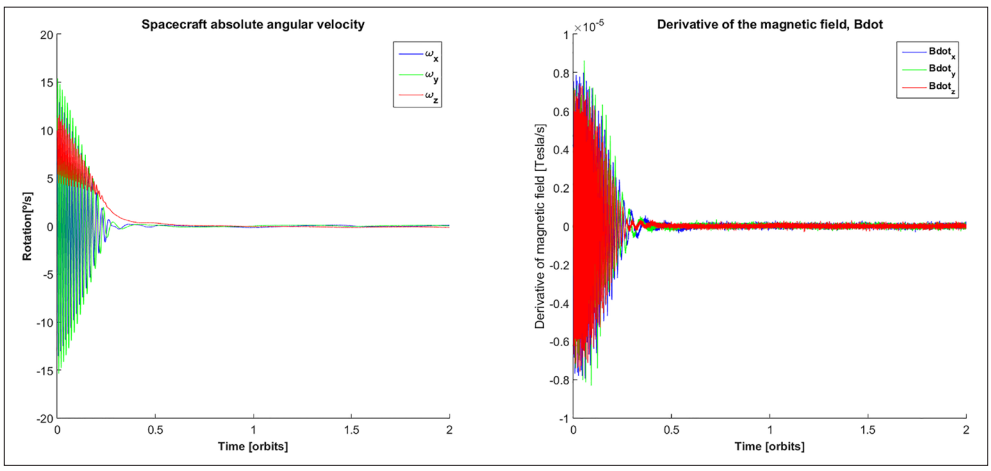

Figure 4 - Simulation of the Bdot controller.

Sun-safe control

The Sun-safe control aims at pointing face of maximum area containing solar cells, placed on the negative z-axis of the satellite, in the direction of the Sun vector within an accuracy of 20º (3σ). Figure 5 shows the performance of the PD-like Sun-safe controller discussed in section "Attitude control". The simulation was carried out with random initial attitude and an initial angular rate of 0.5 º/s per axis. During eclipse the actuators are turned off, since solar information to compute the sun vector from photodiodes is not available. As expected, the angular error increases in eclipse regions where no control torque is generated, and the external disturbances are not counteracted. In regions of sunlight, the magnetorquers are activated, and bring the satellite to the desired attitude within a tolerance of 20º. Nevertheless, the controller takes some time to reach pointing accuracies below the required tolerance after leaving eclipse cycles. Additionally, several simulations were performed and results indicate that this PD control law is very sensitive to control gains, decreasing the overall robustness of the controller.

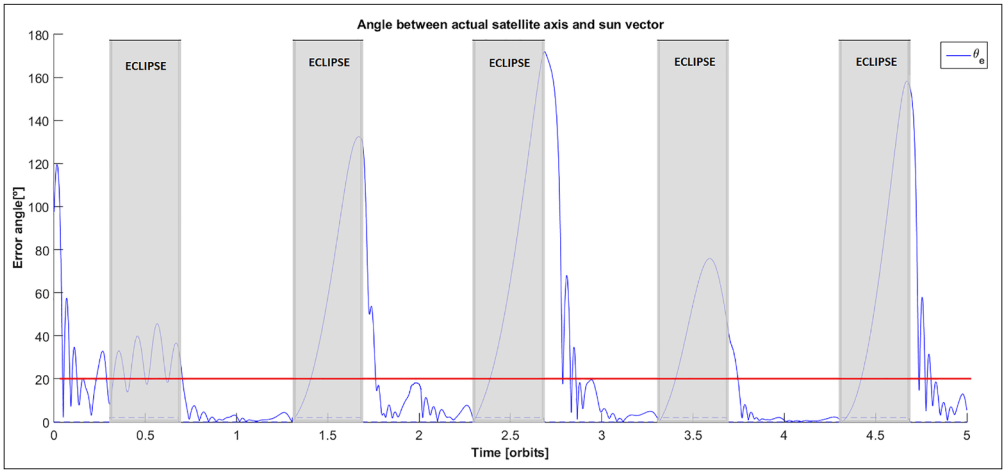

Figure 5 - Simulation of the Sun-safe control mode.

Nominal control

The control law implemented for the nominal mode also uses a PD-like structure, but the proportional term uses the attitude error quaternion. As in the Sun-safe case, the initial attitude is random and the initial angular rate is 0.5º/s per axis. In this case, several simulations with randomized control gains were carried out in order to obtain regions of stability achieving the required pointing performance (7.5º). However, no acceptable results have been found so far using the proposed PD control law and magnetic actuation (Fig. 6). Apart from underactuation issues and the fact that the nadir direction is constantly changing as seen from the satellite, one possible reason for these results is because the desired attitude (axis with maximum moment of inertia pointing towards nadir) is unstable in terms of gravity gradient disturbances. This might affect the overall stability of the system about the target attitude. Nevertheless, further work must be done before discarding this controller for this application.

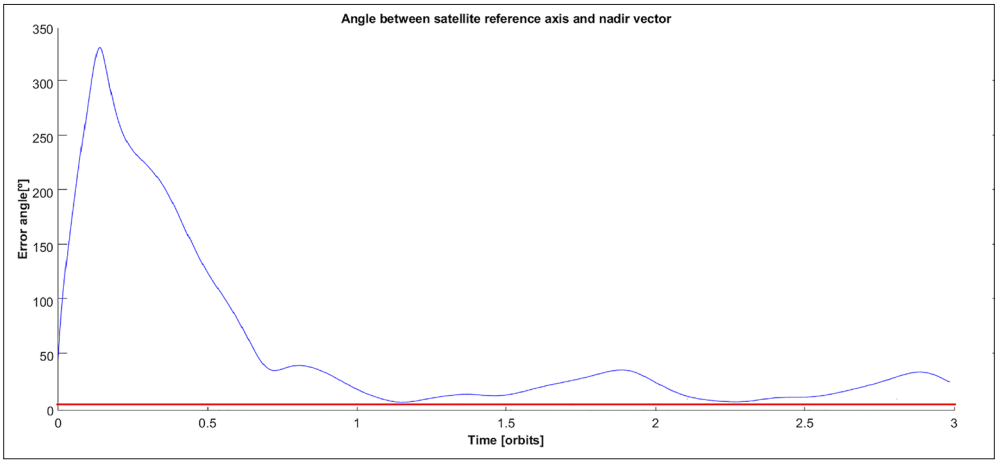

Figure 6 - Simulation of the nominal control mode.

Testing facilities

The following section describes the ADCS testing facilities and equipment available at the NanoSat Lab which is located at the Technical University of Catalonia (BarcelonaTech). The experimental tests are aimed at ensuring the correct functioning of the different ADCS components, validating the attitude determination and control algorithms implemented on-board, calibrating the sensors and actuators, and determining the mass properties of the satellite.

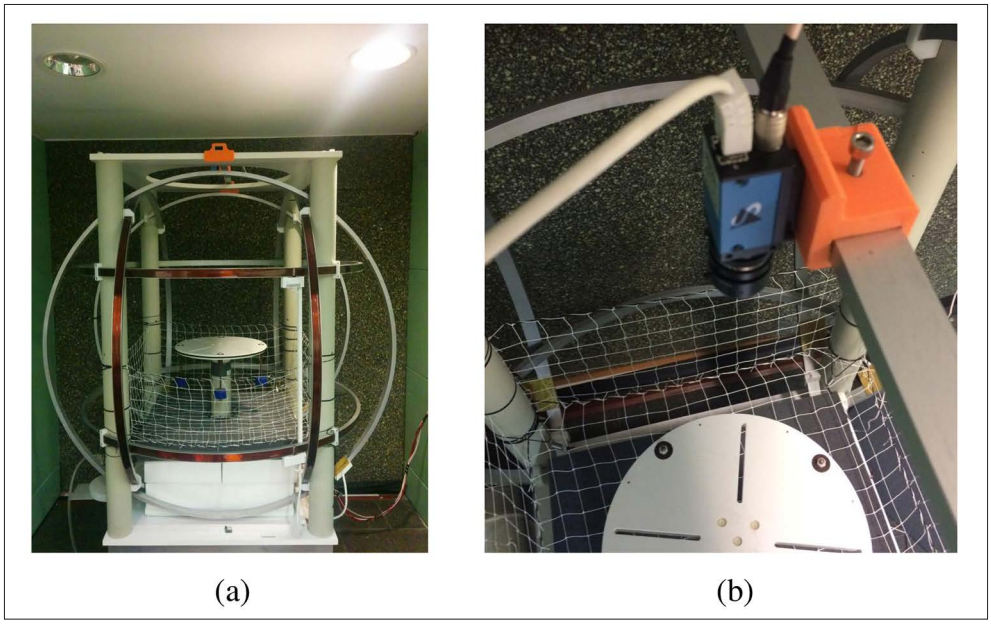

Figure 7 - (a) 3-axis Helmholtz coils and air bearing testbed platform. (b) Optical traking system.

A set of three orthogonal Helmholtz coils along with a spherical air bearing test bed platform and a simple optical tracking system will be used in order to validate the attitude dynamics of ^{3}Cat-2 (Fig. 7). Since the full attitude degrees of freedom are not possible with this kind of system, the tests will be reduced down to a single-axis rotation (vertical axis). The angle as well as the angular rate of the vertical axis will be computed using a computer vision camera that will measure the position of a led placed onto the platform.
The 3-axis Helmholtz coils are aimed at generating the desired magnetic field whereas the air bearing test bed platform is used to simulate the rotational dynamics under reduced friction by a high-pressure air flow impinging on the spherical base of the platform.
Another important parameter for the attitude control system is the inertia of the satellite. The inertia will be computed through two approaches: a computer aided design (CAD) model and an experimental approach. For the experimental determination of the three moments of inertia, a trifilar pendulum was designed. The trifilar pendulum consists of one circular base attached to three steel wires which are separated 120 degrees from each other, and clamped to the ceiling of the lab. Once the satellite is placed onto the base of the pendulum, the moments of inertia can be estimated by measuring the period of oscillation that the platform undergoes when a tiny perturbation is induced. Figure 8 shows the apparatus and the satellite placed onto its base for determining the moment of inertia related to the z-axis. Additionally, this apparatus will also be used to estimate the center of mass of the satellite through three dynamomenters hanging from the three steel wires. The unbalance between dynamometers provides the information needed to locate the center of the mass.

Figure 8 - (a) Trifilar pendulum and ^{3}Cat-2 EM model, without solar panels. (b) Pendulum and dynamometers setting.

Conclusions

This work presented the attitude determination and control system of the ^{3}Cat-2 nanosatellite aimed at testing novel GNSS-R concepts for an Earth Observation mission. The satellite has three ADCS modes of operation: detumbling, Sun-safe, and nominal.
The first one employs the so-called B-dot control law, based on the derivative of the Earth's

local magnetic field to decrease the angular rate of the spacecraft after deployment from the launch vehicle. The simulations performed so far and results presented in section "Results" indicate that this type of control is very robust and suitable for this application, since it is capable of reducing the satellite's angular rate from 10º/s to below 0.5 º/s in less than an orbital period.

The two pointing control modes, Sun-safe and nominal, use a constant gain PD-like control law to bring the satellite to the desired attitude. On the one hand, the Sun-safe mode employs the QUEST algorithm to obtain the angular rate by means of attitude differentiation. This information, along with an estimation of the sun vector, is fed into the controller to compute the torque needed to point the negative z-axis towards the Sun. The simulations presented indicate that the controller takes some time to meet the pointing requirements of 20º after leaving the eclipse region, where the actuators are turned off. However, the overall performance is very sensitive to the control gains resulting in a loss of robustness. An improvement of the system response and pointing performance could be achieved by using spin-stabilization control by means of spinning the face of largest moment of inertia once oriented towards the Sun, or using other control techniques such as a Linear Quadratic Regulator.

On the other hand, the proposed quaternion-based PD control law for the nadir-tracking case does not seem to be suitable for this application, since it results in large pointing errors and do not meet the pointing requirements of 7.5º. Apart from the effects of underactuation and the instantaneous loss of control of one axis, stabilization about an unstable orientation (with respect to the gravity gradient disturbance), where the axis of maximum moment of inertia points towards nadir, might affect dramatically the control performance. Another possible cause of such results might be related to an inappropriate selection of the control gains, since they were chosen empirically. Again, an alternative to the proposed PD control law would be the use of a Linear Quadratic Regulator, or more advanced control techniques. In any case, further research must be conducted before implementing the final algorithms in the on-board computer.

Notation

A: (in bold and upper-case letter) Denotes matrices
a: (in bold and lower-case letter) Denotes vectors
$\mathbf{a}^{b}$**:** Vector **a** expressed in frame b
$\hat{\mathbf{a}}$: Unit vector
$\mathbf{I}_{3x3}$**:** Identity matrix

$$\left[\mathbf{a}^{x}\right]=\begin{bmatrix} 0 & a_3 & -a_2 \\ a_3 & 0 & a_1 \\ a_2 & -a_1 & 0 \end{bmatrix}$$: Skew symmetric matrix based on vector **a**

I: Inertia tensor of the spacecraft
$\mathbf{q}_v$, q_4**:** Vector and scalar parts of the attitude quaternion
$\boldsymbol{\omega}_{ab}^{c}$: Angular rate vector between frame a and b expressed in frame c
$\boldsymbol{\omega}_r$: Spacecraft angular rate vector relative to the orbital LVLH frame
$\mathbf{q}_a^b$: Attitude quaternion representing the rotation of frame b with respect to frame a
A(q): Attitude matrix based on quaternion **q**
μ: Earth's gravitational parameter
$\mathbf{m}_c$: Magnetic moment provided by the magnetorquers

$\mathbf{r}_m$: Reference vector provided by a mathematical model
$\mathbf{s}_m$: Measurement vector provided by the sensors
Δt: Time interval between to measurements
$\mathbf{K}_p$, $\mathbf{K}_d$: Proportional and derivative constant gain matrices
b: Local geomagnetic field vector

Acknowledgements

This project has received funding from the project "Aplicaciones avanzadas en radio ocultaciones y dispersometría utilizando señales GNSS y otras señales de oportunidad" of the Spanish Ministerio de Economia y Competitividad (MINECO), grant no AYA2011-29183-C02-01, the European Union's Seventh Framework Programme for research, technological development and demonstration under grant agreement "European GNSS-R Environmental Monitoring" no FP7-607126-E-GEM, ICREA Acadèmia 2015 award of the Generalitat de Catalunya, and UPC Internal Funds.
We also thank to the GFZ staff, Rolf Köni as TLE expert for ^{3}Cat-2 TLE generation, Carsten Falck as providing NYA satellite receiving station managing, and to Frank Flecthner the GFZ section leader.

References

Avanzini G., Giulietti F. (2012) - *Magnetic Detumbling of a Rigid Spacecraft*. Journal of Guidance, Control, and Dynamics, 35 (4): 1326-1334. doi: http://dx.doi.org/10.2514/1.53074.

Bhat S.P., Dham A.S. (2003) - *Controllability of spacecraft attitude under magnetic actuation*. IEEE Proceedings of Conference on Decision and Control, 3: 2383-2388.

Carreno H., Camps A., Jové R., Alonso A., Olivé R., Amèzaga A., Vidal D., Munoz J.F. (2014) - *The ^{3}Cat-2 project: GNSS-R In-Orbit demonstrator for earth observation*. Proceedings of the 2014 ESA Small Satellites, Systems and Services Symposium, Mallorca, Spain.

Carreno-Luengo H., Camps A., Via P., Munoz J.F., Cortiella A., Vidal D., Jané J., Catarino N., Hagenfeldt M., Palomo P., Cornara S. (2015) - *^{3}Cat-2-An Experimental Nanosatellite for GNSS-R Earth Observation: Mission Concept and Analysis*. IEEE Journal of Selected Topics in Applied Earth Observations and Remote Sensing, PP (99): 1-12. doi: http://dx.doi.org/10.1109/JSTARS.2016.2574717.

Crassidis J.L., Junkins J.L. (2011) - *Optimal estimation of dynamic systems*. Chapman and Hall/CRC press.

Franquiz F.J., Edwards P., Udrea B., Nayak M.V., Pueschl T. (2014) - *Attitude Determination and Control System Design for a 6U CubeSat for Proximity Operations and Rendezvous*. AIAA/AAS Astrodynamics Specialist Conference, SPACE Conferences and Exposition.

Hughes P.C. (2004) - *Spacecraft Attitude Dynamics*. Dover Publications, INC, New York.

Larson W.J., Wertz J.R. (1992) - *Space mission analysis and design*. Microcosm, Inc. Torrance, CA (US). doi: http://dx.doi.org/10.1007/978-94-011-2692-2.

Lovera M., Astolfi A. (2004) - *Spacecraft Attitude Control Using Magnetic Actuators*. IFAC Journal Automatica, 40: 1405-1414. doi: http://dx.doi.org/10.1016/j.automatica.2004.02.022.

Lovera M., Astolfi A. (2006) - *Global magnetic attitude control of spacecraft in the presence of gravity gradient*. IEEE Transactions on Aerospace and Electronic Systems, 42 (3):

796-805. doi: http://dx.doi.org/10.1109/TAES.2006.248214.

Markley F.L., Crassidis J.L. (2014) - *Fundamentals of Spacecraft Attitude Determination and Control*. Springer-Verlag New York. doi: http://dx.doi.org/10.1007/978-1-4939-0802-8.

Murrell J.W. (1978) - *Precision attitude determination for multimission spacecraft*. Proceedings of the AIAA Guidance, Navigation, and Control Conference, Palo Alto, CA, USA. doi: http://dx.doi.org/10.2514/6.1978-1248.

Reyhanoglu M., Drakunov S. (2008) - *Attitude Stabilization of Small Satellites Using Only Magnetic Actuation*. Proceedings of IEEE Industrial Electronics Society, pp. 103-107. doi: http://dx.doi.org/10.1109/iecon.2008.4757936.

Reyhanoglu M., Ton C., Drakunov S. (2009) - *Attitude Stabilization of a Nadir-Pointing Small Satellite Using Only Magnetic Actuators*. Proceedings of IFAC International Conference on Intelligent Control Systems and Signal Processing, pp.1-6. doi: http://dx.doi.org/10.3182/20090921-3-tr-3005.00052.

Shuster M.D., Oh S.D. (1981) - *Three-axis attitude determination from vector observations*. Journal of Guidance, Control, and Dynamics, 4 (1): 70-77. doi: http://dx.doi.org/10.2514/3.19717.

Silani E., Lovera M. (2005) - *Magnetic spacecraft attitude control: a survey and some new results*. Control Engineering Practice, 13 (3): 357-371. doi: http://dx.doi.org/10.1016/j.conengprac.2003.12.017.

Starin S., Bourkland K. (2007a) - *Guaranteeing Pointing Performance of the SDO Sun-Pointing Controllers in Light of Nonlinear Effects*. Proceedings of 20th International Symposium on Space Flight Dynamics, held in Annapolis, MD, 24-28.

Starin S., Bourkland K. (2007b) - *Persistent Attitude Error in a Sun-Pointing Controller due to Nonlinear Dynamics*. AIAA Guidance, Navigation and Control Conference and Exhibit, Guidance, Navigation, and Control and Co-located Conferences. doi: http://dx.doi.org/10.2514/6.2007-6730.

Stickler A.C., Alfriend K.T. (1976) - *Elementary magnetic attitude control System*. Journal of spacecraft and rockets, 13 (5): 282-287. doi: http://dx.doi.org/10.2514/3.57089.

Whaba G. (1965) - *A least squares estimate of spacecraft attitude*. SIAM Review, 7 (3): 409. doi: http://dx.doi.org/10.1137/1007077.

Wie B., Weiss H., Arapostathis A. (1998) - *Quarternion feedback regulator for spacecraft eigenaxis rotations*. Journal of Guidance, Control, and Dynamics, 12 (3): 375-380. doi: http://dx.doi.org/10.2514/3.20418.